Radar-Immune: Enabling Radar-to-Radar Parallel Interference Cancellation using Phase Modulation

***Abstract*—Millimeter-wave sensing has found widespread applications, benefiting numerous individuals worldwide. However, it is vulnerable to interference in real-world environments. Existing efforts have primarily focused on avoiding radar-to-radar (R2R) parallel interference through parameter hopping, with limited attention given to canceling such kind of interference. In this paper, we present Radar-Immune, a novel parallel interference cancellation system. Radar-Immune leverages phase modulation of two chirp sequences, effectively distinguishing the interfering signal from the reflected signal in the Doppler domain. Additionally, we introduce an intersection algorithm to cancel parallel interference. We implement Radar-Immune and conduct performance evaluations for interference cancellation. Experimental results demonstrate an impressive interference cancellation rate of up to 97%. Furthermore, we assess the usability and robustness of Radar-Immune in various real-world scenarios.**

***Index Terms*—Radar-to-radar interference, Millimeter wave radars, Interference cancellation.**

I. Introduction

Millimeter-wave (mmWave) radars are widely used in autonomous vehicles (AVs) due to their excellent range resolution and resilience to changing lighting conditions and adverse weather [2], [20]. The Frequency-Modulated Continuous Wave (FMCW) waveform is commonly employed in mmWave radar systems. However, this waveform is susceptible to interference.

Radar systems can experience interference from multipath signals caused by the environment. Existing work relies on prior information of reflection geometry and training datasets to cancel multipath signals [6], [13]. However, when multiple radars transmit simultaneously, radar-to-radar (R2R) interference can occur. The interfering signal transmitted by other radars can be mistaken by the radar as reflected signals, resulting in the creation of "ghost" objects. These ghost objects pose significant security threats to applications such as smart homes and autonomous driving.

To mitigate R2R interference, existing studies often use parameter hopping techniques to avoid interference [3], [9], [10], [14]. However, parameter hopping is limited by available resources. For instance, frequency hopping-based approaches require a wide bandwidth to enable adjustments in the radar's frequency band. However, radar signals themselves require significant bandwidth for accurate sensing. Consequently, when confronted with numerous interferences, it becomes impractical to identify a frequency band free from interference.

Alternatively, several works focus on canceling interference caused by other radars rather than avoiding it. These systems rely on the assumption that the interfering signal only affects a portion of the received signal and cancels that portion to reconstruct the signal [5], [12], [15], [21], [23]. However, these approaches are effective only when the interfering radar exhibits a different frequency slope compared to the working radar. If both radars share the same frequency slope, the interfering signal, which refers to R2R parallel interference, will impact the entire received signal, rendering these approaches unable to cancel the interference.

Can R2R parallel interference be canceled instead of just mitigating it through parameter hopping? Our key insight lies in differentiating the sources of the interfering signal and the reflected signal. The interfering signal originates from other radars, while the reflected signal is transmitted by our radar. To make the reflected signal distinct from the interfering signal when they share the same parameter setting, we propose introducing differences in the transmitted signal. Building upon this insight, we present Radar-Immune, a novel parallel interference cancellation system that transmits different signal patterns to differentiate the interfering signal from the reflected signal.

Our work addresses two main challenges. The first challenge is to make the reflected signal different from the interfering signal. By manipulating the phase variance in the transmitted signal, we can introduce an additional speed component to objects derived from the reflected signal [24]. This unique phase variance in the transmitted signal ensures that objects derived from the interfering signal do not acquire this additional speed. This insight enables differentiation between the reflected signal and the interfering signal.

The second challenge is to cancel the interference and recover the information in the reflected signal. To achieve this, we design two chirp sequences with different phase variances and calibrate the phase variances when we receive the signal, ensuring the correct information recovery. Such a scheme also guarantees that objects derived from the reflected signal exhibit the same velocity when transmitting these sequences. On the other hand, objects derived from the interfering signal show different velocities due to the phase calibration. This insight allows us to calculate the intersection between the two sets of results, effectively canceling the impact of the interfering signal and recovering accurate information.

In this paper, we introduce Radar-Immune as the first R2R parallel interference cancellation system. Unlike previous approaches that rely on parameters hoping to avoid interference, our system offers a practical solution for canceling parallel interference, making it feasible to implement on commercial off-the-shelf (COTS) radars rather than being limited to theo-

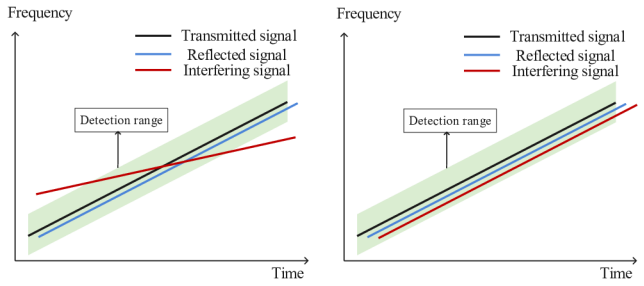

(a) Sweeping interference. (b) Parallel interference.

Fig. 1. The time-frequency signal of the sweeping interference and parallel interference. These interference cause different impacts on mmWave radar sensing. The radar's detection range is represented and visualized by a designated green region.

retical simulations.

We summarize our contributions as follows:

- In this paper, we introduce Radar-Immune as the first R2R parallel interference cancellation system. Unlike previous approaches that rely on parameters hoping to avoid interference, our system offers a practical solution for canceling parallel interference, making it feasible to be implemented on COTS radars rather than being limited to theoretical simulations.
- We present a phase modulation scheme to separate the interfering signal from the reflected signal in the Doppler domain and devise an intersection algorithm using two chirp sequences to cancel parallel interference.
- Furthermore, we implement a prototype of Radar-Immune using the TI AWR1843 platform and evaluate its performance, achieving an impressive interference cancellation rate of up to 97%. We also assess the system's robustness under various conditions, including distance, direction, and multiple interference.

II. Preliminaries

In this section, we first introduce the basic principle of using FMCW radar to detect objects. We then analyze different R2R interference.

A. Principle of FMCW Radar

FMCW radar transmits linearly frequency-modulated signals over time, and the most commonly used signal is a chirp signal.

The FMCW radar transmits a chirp $s(t)$:

$$s(t) = e^{j(2\pi f_L t + \pi S t^2)}, \quad kT_c \le t < (k+1)T_c, \quad k = 0, 1, \cdots, N-1, \tag{1}$$

where f_L is the start frequency, S is the frequency slope, T_c is the chirp period, and N is the total number of chirps.

Suppose there is an object at distance d_i with velocity v_i from the radar, the time delay τ_i can be simplified as $\tau_i = 2d_i/c$, where c is the speed of light. Once the receiver receives the signal, the received signal $r(t)$ is then

$$r(t) = e^{j(2\pi f_L (t-\tau_i) + \pi S (t-\tau_i)^2)}, \quad kT_c \le t < (k+1)T_c, \quad k = 0, 1, \cdots, N-1. \tag{2}$$

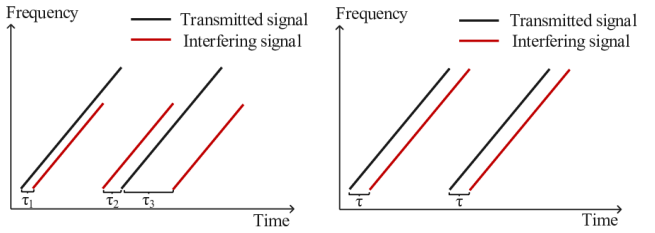

(a) Unstable interference: different period. (b) Stable interference: same period.

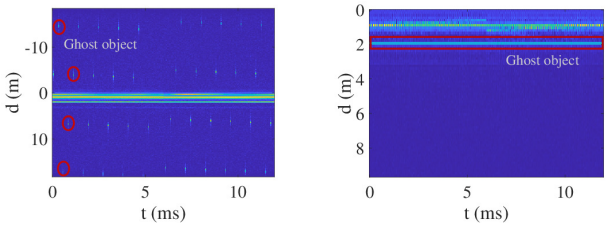

(c) Unstable interference. (d) Stable interference.

Fig. 2. Unstable interference and stable interference: Depending on the chirp period of the transmitted signal and the interfering signal.

The receiver multiplies the transmitted signal $s(t)$ with the conjugation of the received signal $\overline{r(t)}$ to obtain the intermediate frequency (IF) signal $y(t)$:

$$y(t) = s(t) \cdot \overline{r(t)} = \alpha_i e^{j(f_i t + \phi_i)}, \quad kT_c \le t < (k+1)T_c, \quad k = 0, 1, \cdots, N-1. \tag{3}$$

where α_i is the amplitude, and the frequency f_i is related to the time delay τ_i, $f_i = -2\pi S\tau_i$. Fast Fourier Transform (FFT) of the IF signal $y(t)$ can be used to get the spectrum and calculate the frequency. We can estimate the distance by $\hat{d}_i = c\tau_i/2$. This process is defined as range FFT.

To measure the velocity v_i, we calculate the phase difference between adjacent chirps $\Delta\phi = 4\pi v_i T_c/\lambda$, where λ is the wavelength of the FMCW signal. By applying FFT on the slow time, we can get the phase difference across adjacent chirps, and estimate the velocity by $\hat{v}_i = \lambda\Delta\phi/4\pi T_c$. This process is defined as Doppler FFT.

B. R2R Interference

The radar usually has a detection range, which is limited by the low pass filter and transmission power. If the interfering signal transmitted by other radar falls within the detection range of a radar, as shown in Fig. 1, the radar will mistake such interfering signal as its own reflected signal, which causes R2R interference.

R2R interference encompasses sweeping interference and parallel interference, depending on the frequency slope of the interfering signal [11].

Sweeping interference results from a disparity in frequency slope between the transmitted and interfering signals, as shown in Fig. 1(a), leading to an elevation in the effective noise floor and a reduction in radar sensitivity. Conversely, parallel interference occurs when the transmitted signal exhibits an identical frequency slope to the interfering signal, as shown in Fig. 1(b), giving rise to ghost targets that cannot be differentiated from real targets. Consequently, parallel interference

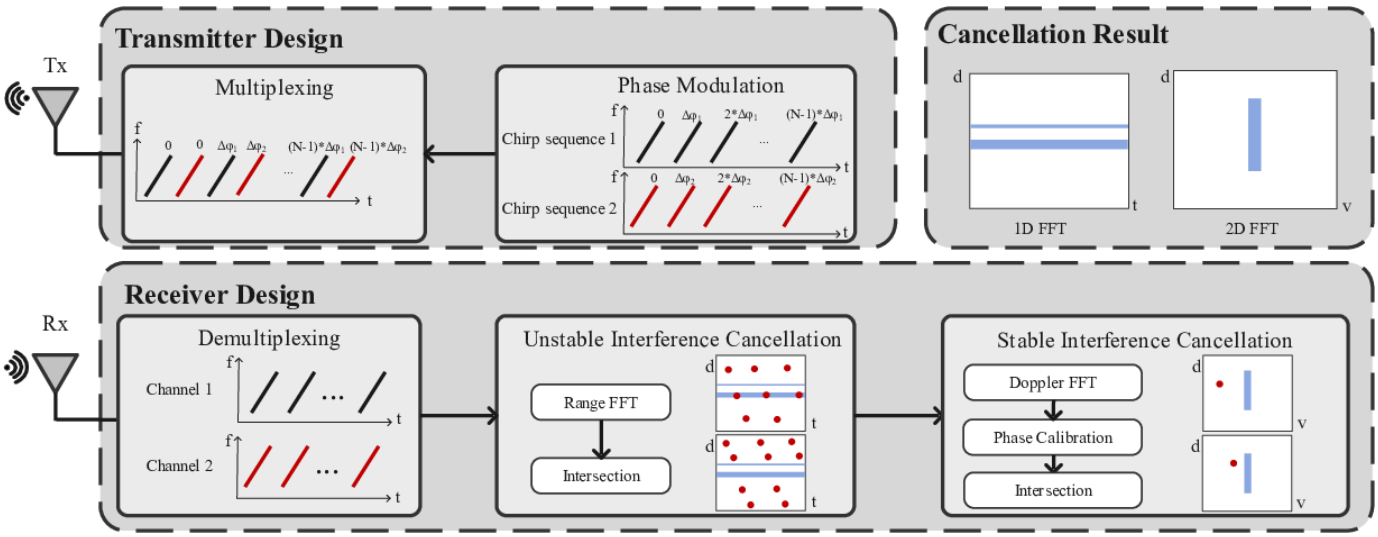

Fig. 3. System architecture. Ghost targets are indicated by the red circle, while real targets are indicated using the color blue in range FFT and Doppler FFT.

poses a more severe security threat for mmWave radars. In this paper, we focus on canceling parallel interference.

III. System Overview

We present Radar-Immune, a system designed to effectively cancel parallel interference in FMCW radars by transmitting different signal patterns to differentiate the interfering signal from the reflected signal. Parallel interference can be categorized into unstable and stable interference based on their chirp period. Unstable interference, as depicted in Fig. 2(a), results in ghost objects appearing at varying distances across consecutive chirps as shown in Fig. 2(c), while stable interference, as depicted in Fig. 2(b), leads to consistent ghost objects over time as shown in Fig. 2(d).

To cancel unstable interference, we leverage the observation that ghost objects move to different positions in adjacent chirps. By comparing distances measured in consecutive chirps, we can effectively cancel unstable interference.

However, canceling stable interference poses greater challenges as it creates persistent ghost objects. To address this, we introduce phase modulation in the transmitted signal to distinguish ghost objects derived from interfering signals from real objects derived from reflected signals in the Doppler domain. This allows for the effective separation and cancellation of stable interference.

The system architecture, as shown in Fig. 3, employs chirp sequences modulated with different phase variances for interference cancellation. The transmitter modulates chirp sequences using varying phase variances and uses time-division multiplexing (TDM) to transmit these chirp sequences alternately. At the receiver, the received signals are demultiplexed into separate channels, each containing different signal patterns. This differentiation enables us to effectively cancel the interfering signal from the reflected signal. Based on the behavior of the interfering signal in the range domain and Doppler domain, we design a cancellation algorithm for unstable and stable interference, respectively. This allows us to cancel the impact of both types of interference and recover accurate radar measurements.

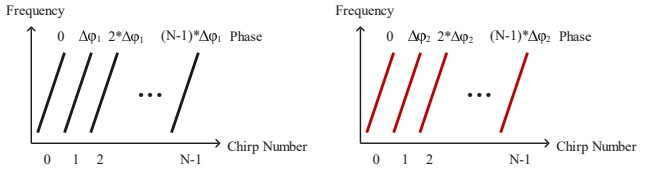

(a) Channel 1: phase variance $\Delta\phi_1$. (b) Channel 2: phase variance $\Delta\phi_2$.

Fig. 4. Two channels are modulated with different phase variances.

IV. Transmitter Design

A. Phase Modulation

To cancel the parallel interference, we should make the transmitted signal different from the interfering signal. Existing radars measure velocity by the phase difference of the chirp sequence [16]. Based on this observation, we propose to modulate phase variance on transmit chirps so that we can "add a speed" to the reflected signal.

In Radar-Immune, we deviate from the conventional FMCW radar transmission system where the initial phase of each chirp is the same. Instead, we introduce different initial phases to each chirp to distinguish the reflected signal from the interfering signal effectively.

To achieve this, we generate two chirp sequences, as depicted in Fig. 4. In the first chirp sequence, we introduce phase variances $\Delta\phi_1$ between adjacent chirps. Similarly, in the second chirp sequence, we incorporate phase variances $\Delta\phi_2$ between adjacent chirps. Subsequently, we transmit these two chirp sequences alternatively.

Suppose the frequency of the transmitted signal is $f_t = S * t + f_0$, where S is the frequency slope, and f_0 is the start frequency, we formulate the chirp sequences $s_1(t)$ and $s_2(t)$ as follows:

$$s_1(t) = Ae^{-j(2\pi f_t t + k_1 \Delta\phi_1)}, \; k_1 T_c \le t < (k_1+1)T_c, \quad k_1 = 0, 1, \cdots, N-1, \tag{4}$$

$$s_2(t) = Ae^{-j(2\pi f_t t + k_2 \Delta\phi_2)}, \; k_2 T_c \le t < (k_2+1)T_c, \quad k_2 = 0, 1, \cdots, N-1, \tag{5}$$

where A is the amplitude of the transmitted signal, T_c is the chirp period, and N is the total number of chirps in each chirp sequence.

B. Multiplexing

To transmit these chirp sequences alternatively, we leverage TDM. Using TDM, the transmitted signal can be formulated by

$$s(t) = \begin{cases} Ae^{-j(2\pi f_t t + \frac{k}{2}\Delta\phi_1)}, kT_c \le t < (k+1)T_c, \\ \qquad\qquad k = 0, 2, \cdots, 2N-2, \\ Ae^{-j(2\pi f_t t + \frac{k-1}{2}\Delta\phi_2)}, kT_c \le t < (k+1)T_c, \\ \qquad\qquad k = 1, 3, \cdots, 2N-1. \end{cases} \tag{6}$$

We transmit $2N$ total number of chirps in the transmitted signal.

V. Receiver Design

A. Demultiplexing

To cancel the interference, it is essential to analyze the signal model of the received signal and separate the individual chirp sequences using time-division demultiplexing. Let's assume that there are N_r objects, then the time delay caused by objects is denoted as τ_i, $i = 1, 2, \cdots, N_r$. Assume there are N_m interfering signals, then the time delay caused by each interfering signal is denoted as τ_m, $m = 1, 2, \cdots, N_m$, and the phase variances in the interfering signal are represented as $\Delta\phi_{m,1}$ and $\Delta\phi_{m,2}$ in the two chirp sequences, respectively. The received signal, denoted as $r(t)$, comprises both the reflected signal, denoted as $r_{re}(t)$, and the interfering signal, denoted as $r_{in}(t)$. Mathematically, we express this as: $r(t) = r_{re}(t) + r_{in}(t)$. The objective is to effectively separate and cancel the interfering signal from the reflected signal to obtain accurate radar measurements. The reflected signal $r_{re}(t)$ can be represented as follows:

$$r_{re}(t) = \begin{cases} A\sum_i e^{-j(2\pi f_t (t-\tau_i) + \frac{k}{2}\Delta\phi_1)}, \; kT_c \le t < (k+1)T_c, \\ \qquad\qquad k = 0, 2, \cdots, 2(N-1), \\ A\sum_i e^{-j(2\pi f_t (t-\tau_i) + \frac{k-1}{2}\Delta\phi_2)}, \; kT_c \le t < (k+1)T_c, \\ \qquad\qquad k = 1, 3, \cdots, 2N-3. \end{cases} \tag{7}$$

Similarly, the interfering signal r_{in} can be formulated as follows:

$$r_{in}(t) = \begin{cases} A\sum_m e^{-j(2\pi f_t (t-\tau_m) + \frac{k}{2}\Delta\phi_{m,1})}, \; kT_c \le t < (k+1)T_c, \\ \qquad\qquad k = 0, 2, \cdots, 2(N-1), \\ A\sum_m e^{-j(2\pi f_t (t-\tau_m) + \frac{k-1}{2}\Delta\phi_{m,2})}, \; kT_c \le t < (k+1)T_c, \\ \qquad\qquad k = 1, 3, \cdots, 2N-3. \end{cases} \tag{8}$$

The block diagram of the COTS radar [8] is illustrated in Fig. 5. In this system, the received signal is mixed with the reference signal $s'(t)$ without any phase shifting. The reference signal $s'(t)$ can be expressed as:

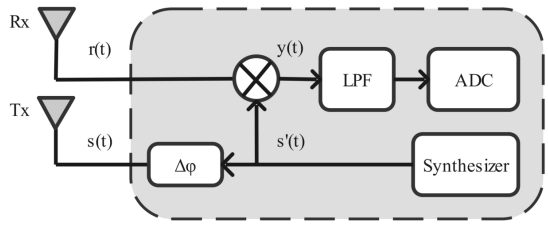

Fig. 5. Block diagram of COTS radar.

$$s'(t) = Ae^{-j2\pi f_t t}. \tag{9}$$

The intermediate frequency (IF) signal $y(t) = s'(t) * \bar{r}(t)$ captures the phase variances $\Delta\phi_1$ and $\Delta\phi_2$, allowing us to separate the interfering signal from the reflected signal. The IF signal comprises the reflected part $y_{re}(t)$ and the interfering part $y_{in}(t)$, i.e., $y(t) = y_{re}(t) + y_{in}(t)$. The reflected part y_{re} can be formulated as follows:

$$y_{re}(t) = \begin{cases} A\sum_i e^{-j(2\pi f_{\tau_i} t - \frac{k}{2}\Delta\phi_1)}, \; kT_c \le t < (k+1)T_c, \\ \qquad\qquad k = 0, 2, \cdots, 2(N-1), \\ A\sum_i e^{-j(2\pi f_{\tau_i} t - \frac{k-1}{2}\Delta\phi_2)}, \; kT_c \le t < (k+1)T_c, \\ \qquad\qquad k = 1, 3, \cdots, 2N-3, \end{cases} \tag{10}$$

where f_{τ_i} is the intermediate frequency related to the time delay τ_i caused by the distance of objects. Besides, the interfering part y_{in} can be expressed as:

$$y_{in}(t) = \begin{cases} A\sum_m e^{-j(2\pi f_{\tau_m} t - \frac{k}{2}\Delta\phi_{m,1})}, \; kT_c \le t < (k+1)T_c, \\ \qquad\qquad k = 0, 2, \cdots, 2(N-1), \\ A\sum_m e^{-j(2\pi f_{\tau_m} t - \frac{k-1}{2}\Delta\phi_{m,2})}, \; kT_c \le t < (k+1)T_c, \\ \qquad\qquad k = 1, 3, \cdots, 2N-3, \end{cases} \tag{11}$$

where f_{τ_m} is the intermediate frequency related to the time delay τ_m caused by the interfering signal.

After applying time-division demultiplexing, we can separate the IF signals into two channels, namely $y_1(t)$ and $y_2(t)$:

$$y_1(t) = \overbrace{A\sum_i e^{-j(2\pi f_{\tau_i} t - k_1\Delta\phi_1)}}^{\text{Reflected part}} + \overbrace{A\sum_m e^{-j(2\pi f_{\tau_m} t - k_1\Delta\phi_{m,1})}}^{\text{Interfering part}}, \quad k_1 T_c \le t < (k_1+1)T_c, k_1 = 0, 1, \cdots, N-1, \tag{12}$$

$$y_2(t) = \overbrace{A\sum_i e^{-j(2\pi f_{\tau_i} t - k_2\Delta\phi_2)}}^{\text{Reflected part}} + \overbrace{A\sum_m e^{-j(2\pi f_{\tau_m} t - k_2\Delta\phi_{m,2})}}^{\text{Interfering part}}, \quad k_2 T_c \le t < (k_2+1)T_c, k_2 = 0, 1, \cdots, N-1. \tag{13}$$

These equations reveal the reflected part and interfering part in each channel, allowing for further processing and effective interference cancellation.

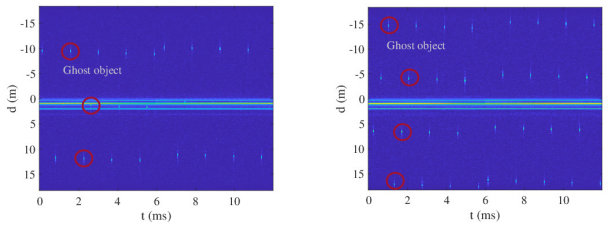

(a) Range FFT for channel 1. (b) Range FFT for channel 2.

Fig. 6. Range FFT for channel 1 and channel 2, which shows how distance changes with the chirp index.

B. Unstable Interference Cancellation

Unstable interference occurs when the chirp period of the interfering signal differs from that of the transmitted signal, leading to varying time delays, as illustrated in Fig. 2(a). In this scenario, the receiver may incorrectly identify the interfering signal as the reflected signal, and the variable time delays $\tau_m = \tau_1, \tau_2, \tau_3 \cdots$ result in the creation of ghost objects at different distances across adjacent chirps.

Based on this insight, we cancel the unstable interference in the range domain by comparing distances with time. Specifically, we apply the range FFT on each chirp of the IF signals $y_1(t)$ and $y_2(t)$ and organize their range FFT results based on the chirp index. The range FFT results for a frame are shown in Fig. 6, illustrating how distance changes with time within the frame. In Fig. 6(a) and Fig. 6(b), we mark the location of the ghost object created by the interfering signal using a red circle. Notably, the location of the ghost target is different in channel 1 and channel 2 due to the alternative transmission of the chirp sequences in adjacent chirps. This behavior aligns with the variable time delays $\tau_1, \tau_2, \tau_3 \cdots$, as depicted in Fig. 2(a). However, the trajectory of the real object remains consistent between these two channels since the chirp length is only several microseconds. Within such a short time, the object's location in adjacent chirps should not change. By exploiting these characteristics, we can effectively cancel unstable interference and distinguish real objects from ghost objects caused by the interfering signal.

The insight that a pixel (t_i, d_i) in channel 1 is interfered with by other radars, while the corresponding pixel at the same location (t_i, d_i) in channel 2 remains unaffected, is valuable for canceling the unstable interference. To cancel the unstable parallel interference, we can perform an intersection operation between these two channels in the range domain. By comparing (t_i, d_i) in both channels, we can identify the regions where interference occurs and replace the interference with the unaffected region in another channel. This intersection process enables us to distinguish the ghost objects caused by the interfering signal from the real objects derived from the reflected signal.

Algorithm 1 presents our proposed intersection algorithm, which aims to cancel parallel interference by identifying and replacing the affected regions in each channel with the corresponding unaffected values from the other channel. The algorithm takes two matrices, $\mathbf{X}$ and $\mathbf{Y}$, representing the

Algorithm 1 Intersection algorithm

Input: Matrix $\mathbf{X}$ calculated in channel 1, matrix $\mathbf{Y}$ calculated in channel 2, a threshold D_T for difference judgment.
Output: Matrix $\mathbf{M}$ and $\mathbf{N}$ whose interference has been canceled in channel 1 and channel 2 respectively.

1: $\mathbf{M} \leftarrow \mathbf{X}$, $\mathbf{N} \leftarrow \mathbf{Y}$
2: $\mathbf{D} \leftarrow |\mathbf{X} - \mathbf{Y}|$.
3: **if** CFAR($\mathbf{D}$) $\neq \emptyset$ **then**
4: **for** rows i, lines j in $\mathbf{D}$ **do**
5: **if** $\mathbf{D}_{i,j} > D_T$ **then**
6: $\mathbf{M}_{i,j} \leftarrow \min(\mathbf{X}_{i,j}, \mathbf{Y}_{i,j})$
7: $\mathbf{N}_{i,j} \leftarrow \min(\mathbf{X}_{i,j}, \mathbf{Y}_{i,j})$
8: **end if**
9: **end for**
10: **end if**
11: **return** $\mathbf{M}$, $\mathbf{N}$

FFT results of $y_1(t)$ and $y_2(t)$, respectively, from channel 1 and channel 2. Additionally, a threshold D_T is assigned to determine the difference between these two matrices. The outputs of the algorithm are the interference-canceled matrices, $\mathbf{M}$ and $\mathbf{N}$, for channel 1 and channel 2, respectively.

First, we initialize matrices $\mathbf{M}$ and $\mathbf{N}$ to $\mathbf{X}$ and $\mathbf{Y}$ respectively (line 1). Then we calculate a difference matrix $\mathbf{D}$ by taking the absolute value of the element-wise difference between $\mathbf{X}$ and $\mathbf{Y}$, i.e, $\mathbf{D} = |\mathbf{X} - \mathbf{Y}|$ (line 2). Next, we check if objects can be detected in the difference matrix $\mathbf{D}$ using the Constant False-Alarm Rate (CFAR) algorithm (line 3). When objects are detected (i.e., CFAR result is positive), we traverse the difference matrix $\mathbf{D}$. For each element in $\mathbf{D}$, if the value is larger than the threshold D_T, it indicates an interference region. We replace the corresponding elements in matrices $\mathbf{M}$ and $\mathbf{N}$ with the minimum value from $\mathbf{X}$ and $\mathbf{Y}$ (lines 4-7). In the absence of interference, retain the original values in matrices $\mathbf{M}$ and $\mathbf{N}$. By doing so, we identify the region where interference occurs and replace this region with the unaffected value from another channel. Finally, the interference canceled matrices $\mathbf{M}$ and $\mathbf{N}$ are returned as the output (line 14).

By using the range FFT results shown in Fig. 6 as inputs $\mathbf{X}$ and $\mathbf{Y}$, we can effectively cancel the impact of unstable interference and obtain accurate distance estimations for the real objects.

C. Stable Interference Cancellation

Stable interference arises when the interfering signal's chirp period matches that of the transmitted signal, resulting in a consistent time delay τ being detected by the receiver, as shown in Fig. 2(b). In contrast to unstable interference, where ghost objects can be distinguished in the range domain by comparing the two channels, stable interference poses a more challenging problem. The ghost object created by stable interference remains fixed in distance across chirps, making it impossible to identify and remove solely based on range information. To overcome this limitation, we can explore

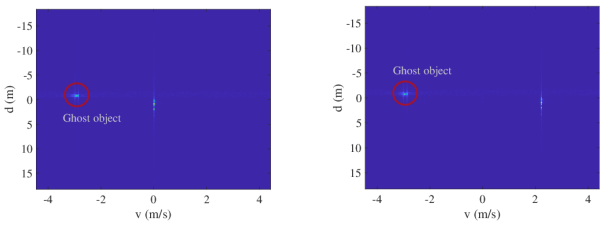

(a) Doppler FFT for the channel 1: $\Delta\phi_1 = 0$. (b) Doppler FFT for the channel 2: $\Delta\phi_2 = -\pi/2$.

Fig. 7. Doppler FFT results when the interference has a stable phase variance in chirps.

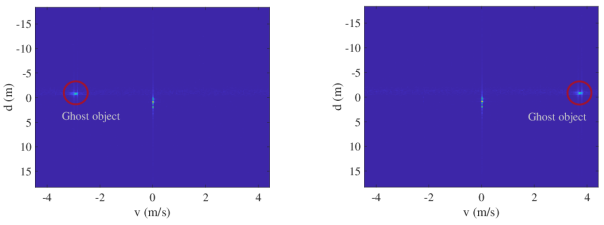

(a) Calibrated Doppler FFT for the channel 1: $\Delta\phi_1 = 0$. (b) Calibrated Doppler FFT for the channel 2: $\Delta\phi_2 = -\pi/2$.

Fig. 8. Phase calibrated Doppler FFT.

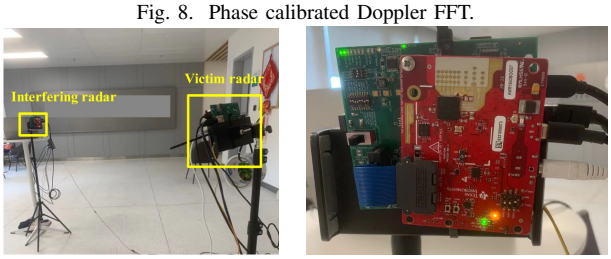

(a) Experiment scenario. (b) TI AWR1843 platform.

Fig. 9. Experiment scenario and hardware platform.

alternative domains to separate the interfering signal from the reflected signal. One potential domain is the Doppler domain.

To cancel the stable interference, we introduce different phase variances to the chirp sequences, imparting a velocity component to the reflected signal while the interfering signal lacks such a velocity component. This strategy enables the separation of the interfering signal from the reflected signal. In FMCW radars, velocity estimation relies on measuring the phase difference in the chirp sequence. Suppose an object is located at a distance d_i from the radar moving at a speed of v_i, the reflected signal has a time delay of $\tau_i = 2(d_i \pm v_i k)/c$, where k is the chirp index and c is the speed of light. By Substitute τ_i to Equ. (12) and Equ. (13), we obtain the phase difference in the adjacent chirps for the reflected part, denoted as $\Delta\phi_{re1}$ and $\Delta\phi_{re2}$ respectively. The phase difference in adjacent chirps of the reflected part for channel 1 $\Delta\phi_{re1}$ and channel 2 $\Delta\phi_{re2}$ can be expressed as $\Delta\phi_{re1} = \frac{4\pi f_t v_i}{c} + \Delta\phi_1$, $\Delta\phi_{re2} = \frac{4\pi f_t v_i}{c} + \Delta\phi_2$.

On the other hand, The time delay of the interfering part τ_m does not have any velocity component, which means that the phase difference in adjacent chirps of the interfering part for both channel 1 $\Delta\phi_{in1}$ and channel 2 $\Delta\phi_{in2}$ is only affected by the phase variance in the signal. Hence, we have $\Delta\phi_{in1} = \Delta\phi_{m,1}$ and $\Delta\phi_{in2} = \Delta\phi_{m,2}$.

Assume phase variances in the interfering signal are static, such that $\Delta\phi_{m,1} = \Delta\phi_{m,2}$, phase modulation in the transmitted signal can "add a different speed" to the reflected signal in two channels. By performing Doppler FFT, we present a Doppler FFT result example when $\Delta\phi_1 = 0$ and $\Delta\phi_2 = -\pi/2$ in Fig. 7. As a result, the reflected signal in each channel acquires a different "speed" when processed through the Doppler FFT. This difference in the "speed" is a consequence of the phase modulation and enables us to differentiate the detected objects calculated from the reflected signal in these two channels. On the other hand, the interfering signal maintains stable phase variances. Consequently, the ghost object calculated from the interfering signal retains its original velocity in both channels, and this enables us to distinguish it from the objects derived from the reflected signal.

To recover the real velocity of real objects, we design phase calibration sequences $c_1(k_1)$ and $c_2(k_2)$ to mitigate the "speed" added to the reflected signal. Specifically, we design a phase calibration sequence $c_1(k_1)$ and $c_2(k_2)$ as follow:

$$c_1(k_1) = e^{-jk_1\Delta\phi_1}, \ k_1 = 0, 1, \cdots, N-1, \tag{14}$$

$$c_2(k_2) = e^{-jk_2\Delta\phi_2}, \ k_2 = 0, 1, \cdots, N-1. \tag{15}$$

By multiplying these phase calibration sequences to $y_1(t)$ and $y_2(t)$ respectively, we effectively calibrate the "speed" that was initially "added" to the reflected signal during the phase modulation process. After the calibration, the phase differences between adjacent chirps in these two channels for the reflected part $\Delta\phi'_{re1}$ and $\Delta\phi'_{re2}$ become:

$$\Delta\phi'_{re1} = \Delta\phi_{re1} - \Delta\phi_1 = \frac{4\pi f_t v_i}{c}, \tag{16}$$

$$\Delta\phi'_{re2} = \Delta\phi_{re2} - \Delta\phi_2 = \frac{4\pi f_t v_i}{c}. \tag{17}$$

After phase calibration, the real objects derived from the reflected signal will maintain their velocities across the channels. However, the phase difference for the interfering part $\Delta\phi'_{in1}$ and $\Delta\phi'_{in2}$ are then:

$$\Delta\phi'_{in1} = \Delta\phi_{in1} - \Delta\phi_1 = \Delta\phi_{m,1} - \Delta\phi_1, \tag{18}$$

$$\Delta\phi'_{in2} = \Delta\phi_{in2} - \Delta\phi_2 = \Delta\phi_{m,2} - \Delta\phi_2. \tag{19}$$

The ghost object will be modulated to different Doppler bands in the two channels, as illustrated in Fig. 8.

This differentiation in the Doppler domain allows us to separate and cancel the stable interference using the intersection algorithm proposed in Algorithm 1. Using the phase-calibrated Doppler FFT results as inputs $\mathbf{X}$ and $\mathbf{Y}$, we can effectively cancel the impact of stable interference and obtain accurate velocity estimations for the real objects.

VI. Evaluation

A. Implementation and Setup

Hardware. We implement Radar-Immune using the Texas Instrument (TI) mmWave sensor AWR1843BOOST and the data capture adapter DCA1000EVM. The AWR1843BOOST works in the 76-81GHz band and is equipped with three transmitter antennas and four receiver antennas. In our experiment, we only use one transmitter antenna and one receiver antenna to show the performance of interference cancellation. Besides, AWR1843BOOST provides a phase-shifting module before transmission, enabling phase modulation in our system. We perform data processing and analysis on a desktop (AMD Ryzen 7 3700X) equipped with an 8-Core Processor @3.60GHz and 16GB of RAM.

Software. We use mmWave Studio to configure mmWave sensor modules and acquire the data from Analog-to-Digital Converter (ADC). Besides, we use MATLAB R2022(a) to read the data and implement our interference cancellation algorithm.

B. Evaluation Metric

We assess the quality of the interference cancellation using the following subjective and objective evaluation metrics.

SSR of Ghost Targets: The signal strength reduction (SSR) of ghost targets is computed as the difference between the estimated amplitudes of the ghost targets after parallel interference cancellation and the corresponding amplitudes computed before interference cancellation. For ghost targets, the larger SSR indicates better performance because Radar-Immune should cancel almost ghost targets.

SSR of Real Targets: The SSR of real targets is computed as the difference between the estimated amplitudes of the real targets after parallel interference cancellation and the corresponding amplitudes computed before interference cancellation. For real targets, the smaller SSR indicates better performance because Radar-Immune does not cancel real targets.

Ghost target cancellation rate (GTCR): This rate evaluates how powerful our system can cancel the ghost object. If objects appear at different positions or velocities in different channels for a certain frame, this frame is labeled to be interfered with by other radars. We count the total number of interfered frames N. After interference cancellation, we use CFAR to check whether these ghost objects have been canceled and count the number of frames M that the ghost object has been successfully mitigated. The ghost object cancellation rate is then M/N.

C. Overall Performance

This experiment aims to assess the overall performance of Radar-Immune and find suitable parameters in the algorithm. We illustrate our experiment setup and TI platform in Fig. 9, one radar is served as interfering radar, and another radar work as victim radar. The sampling rate is set to 20 MHz, and ADC samples of a chirp are 248. We set the same frequency slope of 100 $MHz/\mu s$ for interfering radar and victim radar, and adjust their chirp period to generate unstable interference or stable interference. For unstable interference, we set the chirp period of the victim radar to 18 μs and the chirp period of the interfering radar to 28 μs. For stable interference, we set the chirp period of both radars to 18 μs. We set the threshold D_T to the median value of the difference matrix $\mathbf{D}$ in the intersection algorithm. Meanwhile, we ask a person to walk around to create a real object.

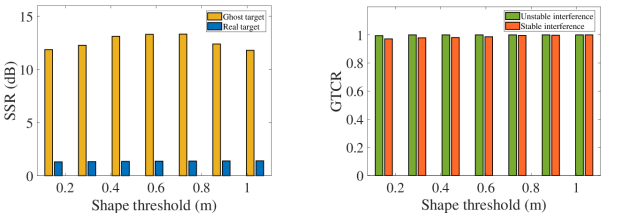

(a) Signal strength reduction. (b) Ghost target cancellation rate.

Fig. 10. Impact of the shape threshold.

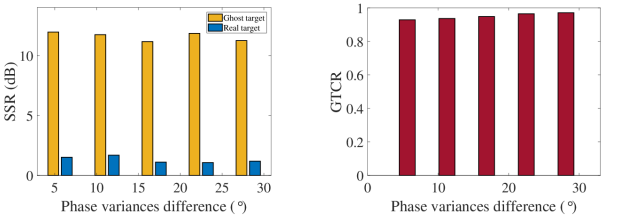

(a) Signal strength reduction. (b) Ghost target cancellation rate.

Fig. 11. Impact of phase variances difference.

We investigate suitable parameters to evaluate interference cancellation. Specifically, we define a *shape threshold*, within this threshold, these detected points by CFAR are regarded as the same object. The *shape threshold* is used as follows: For any points detected in channel i ($i = 1, 2$) using CFAR, if the minimum Euclidean distance between this point and any points detected in channel j ($j \neq i, j = 1, 2$) is smaller than the *shape threshold*, it is labeled as the same real object. Otherwise, it is labeled as a ghost object.

In addition, we investigate the influence of the phase variances introduced to the chirp sequence. Specifically, we define the *phase variances difference* as the difference between the phase variance of the first chirp sequence, and that of the second chirp sequence.

1) Impact of the shape threshold: The relationship between the *shape threshold* and the SSR is illustrated in Fig. 10(a), while the relationship between the *shape threshold* and the GTCR is depicted in Fig. 10(b). The amplitude of ghost objects can be reduced by 12 dB, while that of real objects remains nearly unchanged, as evident in Fig. 10(a). Notably, at a *shape threshold* of 0.3 m, the GTCR for unstable interference reaches 100%, and for stable interference, it achieves 97.09%, with errors primarily attributed to noise. Increasing the *shape threshold* enhances the GTCR for stable interference due to its improved robustness against noise points.

2) Impact of phase variances difference: In this experiment, we investigate the effect of the *phase variances difference* on

TABLE I
PERFORMANCE OF MULTIPLE INTERFERING SOURCES

Scenario	SSR of Ghost Targets	SSR of Real Targets	GTCR
Two stable interferences	11.43 dB	1.41 dB	96.64%
Two unstable interferences	12.31 dB	0.96 dB	99.12%
One stable and one unstable interference	10.71 dB	1.11 dB	95.32%

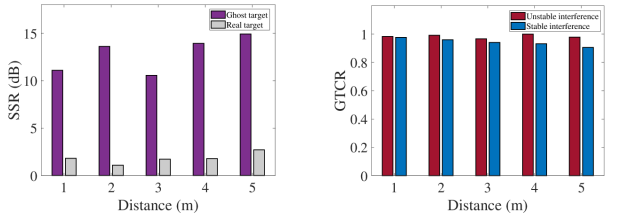

(a) Signal strength reduction. (b) Ghost target cancellation rate.

Fig. 12. SSR and GTCR with various distances.

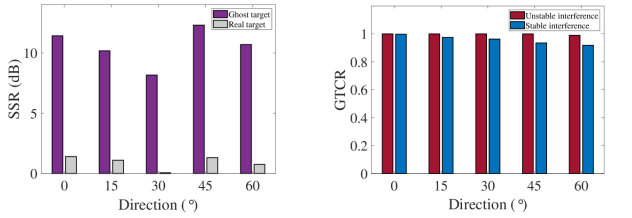

(a) Signal strength reduction. (b) Ghost target cancellation rate.

Fig. 13. SSR and GTCR with various directions.

the system performance. The relationship between the *phase variances difference* and the SSR is presented in Fig. 11(a), while the relationship between the *phase variances difference* and the GTCR is illustrated in Fig. 11(b). The SSR of ghost targets is 12 dB, while that of real targets is within 2 dB for each *phase variances difference*, as observed in Fig. 11(a). Notably, even with the smallest phase variances difference, which is 5.625° provided by the TI AWR1843 radar [8], the GTCR can still achieve 92.88%. As the *phase variances difference* increases, the ghost targets shift farther away from the real targets, making them easier to distinguish, resulting in an increase in GTCR.

D. Robustness Evaluation

In this experiment, we assess the robustness of Radar-Immune across various distances, directions, multiple interfering sources, and moving scenarios.

1) Impact of Distance and Direction: In this experiment, we adjust the distance from 1 m to 5 m at a fixed angle of 0°, and the direction from 0° to 60° at a fixed distance of 1 m. For each distance and direction setting, we generate a stable interference signal or an unstable interference signal.

We report the results of these experiments in terms of SSR and GTCR in Fig. 12 and Fig. 13. Remarkably, Radar-Immune continues to demonstrate good performance even at a distance of 5 m and a direction of 60°. As depicted in Fig. 12(b) and Fig. 13(b), the increasing distance and angle lead to the attenuation of the mmWave signal in Signal-to-Noise Ratio (SNR). However, the SSR for ghost targets is 12.82dB, whereas that for real targets is only 1.82 dB, as illustrated in Fig. 12(a) and Fig. 13(a). GTCR remains unaffected by these changes. In the worst-case scenario, Radar-Immune achieves an average GTCR of 96.64% for unstable interference and 90.58% for stable interference, showcasing its robustness.

2) Impact of Multiple Interfering Sources: We further evaluate the performance of Radar-Immune with multiple interfering sources. The experimental setup involves the deployment of two radars as interfering sources, while a third radar serves as the victim radar. The interfering radars are configured to generate specific interference patterns, including two stable interferences, two unstable interferences, and a combined scenario with one stable and one unstable interference.

The experimental results are summarized in Table I. Specifically, in a scenario involving one stable and one unstable interference, the SSR of the ghost targets achieved an impressive 10.71 dB, while that of the real targets is only 1.11 dB. The GTCR demonstrates a consistently high performance exceeding 95% when confronted with multiple interfering sources. These outcomes collectively attest to the robustness of the Radar-Immune system in the presence of multiple interfering sources, enabling the effective cancellation of both stable and unstable interferences simultaneously.

3) Impact of Moving: In this experiment, we investigate the impact of a moving interfering radar on the performance of Radar-Immune. One user holds an interfering radar and moves towards the victim radar. The results demonstrate that Radar-Immune maintains robustness even with a moving interfering radar. Specifically, the SSR of the ghost targets is 11.53 dB, while that of the real targets is 1.02 dB. Furthermore, the GTCR achieves 99.1% for unstable interference and 97.5% for stable interference, showcasing its effectiveness in canceling interference. These findings highlight the ability of Radar-Immune to effectively distinguish between real targets and interfering radars, even when they are in motion, owing to the alternative transmission of the two chirp sequences, which ensures consistent positions and velocities for real targets across these two channels.

VII. DISCUSSION

We discuss the utilization and cost of Radar-Immune in this section.

Utilization: When the difference between the phase variances of the chirp sequences in the interfering signal and the transmitted signal is the same, meaning that $\Delta\phi_{m,1} - \Delta\phi_{m,2} = \Delta\phi_1 - \Delta\phi_2$, Radar-Immune cannot cancel the interfering signal. How many radars can be supported to transmit simultaneously with interference cancellation ability

using Radar-Immune? As an example, let's consider the TI AWR1843 radar, which supports 64 different phase variances. This means that the radar can accommodate up to 64 different signals transmitted simultaneously using two chirp sequences.

To support more radars operating simultaneously, we can add more chirp sequences. For example, we can use the third chirp sequence with phase variance $\Delta\phi_3$, and use TDM to transmit these three chirp sequences alternatively. If the interfering signal cannot be canceled using two chirp sequences, it is more likely to be canceled using three or more chirp sequences. More chirp sequences with different phase variances also support more radars operating simultaneously using Radar-Immune.

Cost: To cancel the parallel interference, we use multiple chirp sequences and the final result is the intersection of these channels. Therefore, we sacrifice the time efficiency for velocity estimation. Specifically, assume the chirp period is T_c and the wavelength is λ, the maximum relative speed (v_{max}) that can be measured by adjacent chirps spaced T_c apart is $v_{max} = \frac{\lambda}{4T_c}$. Radar-Immune uses $2T_c$ spaced chirps to estimate the velocity, causing a maximum relative speed of $v_{max}/2$. If we use n chirp sequences to support more radars operating simultaneously, the maximum relative speed that Radar-Immune can measure is then v_{max}/n.

Compared to the traditional transmission scheme, our system sacrifice the maximum relative speed that can measure, to obtain a more robust measurement.

VIII. Related Work

This section presents an overview of the current state-of-the-art research related to the mitigation of R2R interference. R2R interference mitigation approaches can be broadly categorized into two main strategies: interference avoidance and interference cancellation.

Interference Avoidance: Many existing works in interference avoidance employ radar parameter hopping techniques, either randomly or in a coordinated manner. For instance, Khoury *et al.* proposed a random frequency hopping scheme to avoid parallel interference [9], and Haritha *et al.* designed a slotted ALOHA and CSMA protocol for parallel interference mitigation [7]. Uysal introduced a phase-coded FMCW radar to mitigate interference [22], which, however, requires complex hardware architecture for sub-chirp encoding and decoding. These approaches can be constrained by limited resources, especially in scenarios with a high density of radar systems and potential interferences. Besides, implementing these techniques is costly, and their evaluation mostly relies on simulation environments.

Some researchers have proposed centralized radar coordination systems to mitigate parallel interference [3], [14]. These systems utilize a central coordinator to instruct individual radars to adjust their parameters for interference mitigation. Nevertheless, the deployment of coordinators can be challenging and costly. As a result, achieving interference cancellation without relying on interference avoidance may be a more practical approach.

Interference Cancellation: Several works have introduced R2R interference cancellation systems, but they only consider sweeping interference rather than parallel interference. The sweeping interference cancellation systems can be classified into two categories based on the treatment of the interfered signal components: (1) *Reduction:* These systems identify the interfered components within a chirp and remove them to mitigate interference. Techniques such as subtraction [1], [17], [21] and Short Time Fourier Transform (STFT) with L statistic [12] have been employed to effectively reduce sweeping interference. (2) *Reconstruction:* These systems aim to compensate for the interfered components and reconstruct the original signal. Various methods, including interpolation-based approaches [5], autoregressive modeling [15], signal decomposition techniques [4], compressed sensing algorithms [23], and deep learning architectures [18], [19], have been explored for sweeping interference mitigation. By utilizing the non-interfered components, these approaches enhance signal recovery and denoising capabilities.

It is essential to note that these sweeping interference cancellation methods are specifically designed to address scenarios where only a portion of a chirp is affected by interference. Therefore, they leverage the unaffected components within the chirp for denoising and signal recovery. However, these methods are not directly applicable to canceling parallel interference, as the interference affects the entire chirp. Unlike sweeping interference, which may primarily reduce sensing capability and increase the noise floor, parallel interference poses a more severe concern in creating ghost objects. Previous research has primarily focused on interference cancellation at the receiver, which limits its ability to cancel the parallel interference. In contrast, Radar-Immune introduces a novel scheme that cancels interference by employing distinct signal patterns during transmission, making it the first system to effectively cancel parallel interference.

IX. Conclusion

This paper proposed Radar-Immune, a novel R2R parallel interference cancellation system that utilizes phase modulation techniques to differentiate the interfering signal from the reflected signal. Unlike conventional approaches that aim to avoid interference, Radar-Immune can effectively cancel parallel interference even in the presence of interference. The extensive evaluation demonstrates the system's efficacy and robustness in real-world scenarios, considering various factors such as distance, direction, multiple interference, and moving scenarios. However, it is important to note that Radar-Immune is specialized for canceling parallel interference and may not address sweeping interference cancellation. For future work, we envision exploring a unified interference cancellation system capable of simultaneously addressing both sweeping interference and parallel interference.

References

[1] M Alhumaidi and M Wintermantel. Interference avoidance and mitigation in automotive radar. In *17th European Radar Conference (EuRAD)*, pages 172–175, 2021.

[2] Szilárd Aradi. Survey of deep reinforcement learning for motion planning of autonomous vehicles. *IEEE Transactions on Intelligent Transportation Systems*, 23(2):740–759, 2020.

[3] Canan Aydogdu, Musa Furkan Keskin, Nil Garcia, Henk Wymeersch, and Daniel W Bliss. Radchat: Spectrum sharing for automotive radar interference mitigation. *IEEE Transactions on Intelligent Transportation Systems*, 22(1):416–429, 2019.

[4] Ashwin Bhobani Baral, Bhaskar Raj Upadhyay, and Murat Torlak. Automotive radar interference mitigation using two-stage signal decomposition approach. In *2023 IEEE Radar Conference (RadarConf23)*, pages 1–6, 2023.

[5] Jonathan Bechter, Fabian Roos, Mahfuzur Rahman, and Christian Waldschmidt. Automotive radar interference mitigation using a sparse sampling approach. In *2017 European Radar Conference (EURAD)*, pages 90–93, 2017.

[6] Evert I Pocoma Copa, Kheireddine Aziz, Maxim Rykunov, Eddy De Greef, André Bourdoux, and François Horlin. Radar fusion for multipath mitigation in indoor environments. In *2020 IEEE Radar Conference (RadarConf20)*, pages 1–5, 2020.

[7] K. Haritha, Vineeth Bala Sukumaran, and Chandramani Kishore Singh. Slotted aloha and csma protocols for fmcw radar networks. *ArXiv*, abs/2201.09030, 2022.

[8] Texas Instruments. Awr1843 single-chip 77 to 79 ghz fmcw radar sensor ti datasheet. https://www.ti.com/lit/gpn/awr18431, 2022.

[9] Joud Khoury, Ram Ramanathan, Dan McCloskey, Russell Smith, and Timothy Campbell. Radarmac: Mitigating radar interference in self-driving cars. In *13th Annual IEEE International Conference on Sensing, Communication, and Networking (SECON)*, pages 1–9, 2016.

[10] Thomas Moon, Jounsup Park, and Seungmo Kim. Bluefmcw: Random frequency hopping radar for mitigation of interference and spoofing. *EURASIP Journal on Advances in Signal Processing*, 2022(1):1–17, 2022.

[11] Robert Muja, Andrei Anghel, Remus Cacoveanu, and Silviu Ciochina. Assessment of rf interference mitigation methods for automotive radars using real data. In *14th International Conference on Communications (COMM)*, pages 1–5, 2022.

[12] Robert Muja, Andrei Anghel, Remus Cacoveanu, and Silviu Ciochina. Interference mitigation in fmcw automotive radars using the short-time fourier transform and l-statistics. In *2022 IEEE Radar Conference (RadarConf22)*, pages 1–6, 2022.

[13] Jeong-Ki Park, Jae-Hyun Park, and Kyung-Tae Kim. Multipath signal mitigation for indoor localization based on mimo fmcw radar system. *IEEE Internet of Things Journal*, 2023.

[14] Yanlong Qiu, Jiaxi Zhang, Kaiyi Huang, Jin Zhang, and Bo Ji. Poster: Radar-ca: Radar-sensing multiple access with collision avoidance. In *Proceedings of the 21st Annual International Conference on Mobile Systems, Applications and Services*, pages 581–582, 2023.

[15] Muhammad Rameez, Mattias Dahl, and Mats I Pettersson. Autoregressive model-based signal reconstruction for automotive radar interference mitigation. *IEEE Sensors Journal*, 21(5):6575–6586, 2020.

[16] Sandeep Rao. Introduction to mmwave sensing: Fmcw radars. https://www.ti.com/content/dam/videos/external-videos/2/3816841626001/5415528961001.mp4/subassets/mmwaveSensing-FMCW-offlineviewing_0.pdf, 2017.

[17] Sandeep Rao and Anil Varghese Mani. Characterization of some interference mitigation schemes in fmcw radar. In *2021 IEEE Radar Conference (RadarConf21)*, pages 1–6, 2021.

[18] Johanna Rock, Mate Toth, Elmar Messner, Paul Meissner, and Franz Pernkopf. Complex signal denoising and interference mitigation for automotive radar using convolutional neural networks. In *22th International Conference on Information Fusion (FUSION)*, pages 1–8, 2019.

[19] Marius Schwarz, Axel Acosta Aponte, and Gor Hakobyan. Deep-learning based spectrum prediction for cognitive automotive radar interference mitigation. In *2023 IEEE Radar Conference (RadarConf23)*, pages 1–6, 2023.

[20] Onur Toker and Suleiman Alsweiss. mmwave radar based approach for pedestrian identification in autonomous vehicles. In *2020 SoutheastCon*, pages 1–2, 2020.

[21] Lizette Lorraine Tovar Torres, Timo Grebner, David Werbunat, and Christian Waldschmidt. Automotive radar interference mitigation by subtraction of the interference component. *IEEE Microwave and Wireless Technology Letters*, 2023.

[22] Faruk Uysal. Phase-coded fmcw automotive radar: System design and interference mitigation. *IEEE Transactions on Vehicular Technology*, 69(1):270–281, 2019.

[23] Yubo Wu, Y Thomas Hou, Alexander Li, and Wenjing Lou. Real-time interference mitigation for automotive radar. In *2023 IEEE Radar Conference (RadarConf23)*, pages 1–6, 2023.

[24] Feng Xu, Sergiy A Vorobyov, and Fawei Yang. Transmit beamspace ddma based automotive mimo radar. *IEEE Transactions on Vehicular Technology*, 71(2):1669–1684, 2021.